
MSGNN: A Spectral Graph Neural Network Based on a Novel Magnetic Signed Laplacian

Yixuan He

University of Oxford

yixuan.he@stats.ox.ac.uk

Michael Perlmutter

University of California, Los Angeles

perlmutter@ucla.edu

Gesine Reinert

University of Oxford

reinert@stats.ox.ac.uk

Mihai Cucuringu

University of Oxford

mihai.cucuringu@stats.ox.ac.uk

Abstract

Signed directed networks are ubiquitous in real-world applications. However, there has been relatively little work proposing spectral graph neural network (GNN) methods for analyzing such networks. Here we introduce a signed directed Laplacian matrix, which we call the magnetic signed Laplacian, as a natural generalization of both the signed Laplacian on signed graphs and the magnetic Laplacian on directed graphs. We then use this matrix to construct a novel spectral GNN architecture and conduct extensive experiments on both node clustering and link prediction tasks. In these experiments, we consider tasks related to signed information, tasks related to directional information, and tasks related to both signed and directional information. We demonstrate that our proposed spectral GNN is effective for incorporating both signed and directional information, and attains leading performance on a wide range of data sets. Additionally, we provide a novel synthetic network model, which we refer to as the signed directed stochastic block model, and a number of novel real-world data sets based on lead-lag relationships in financial time series.

1 Introduction

Graph Neural Networks (GNNs) have emerged as a powerful tool for extracting information from graph-structured data and have achieved state-of-the-art performance on a variety of machine learning tasks. However, the vast majority of research has been on constructing GNNs for unsigned and undirected graphs, and there has been comparatively little work designing GNNs for graphs where the edges have a natural notion of sign and/or direction.

This is unfortunate because many important and interesting phenomena are naturally modeled as signed and/or directed graphs, i.e., graphs in which objects may have either positive or negative relationships, and/or in which such relationships are not necessarily symmetric [1]. For example, in the analysis of social networks, positive and negative edges could model friendship or enmity, and directional information could model the influence of one person on another [2, 3]. Signed/directed networks also arise when analyzing time-series data with lead-lag relationships [4], detecting influential groups in social networks [5], and computing rankings from pairwise comparisons [6]. Additionally, signed and directed networks are a natural model for group conflict analysis [7], modeling the interaction network of the agents during a rumor spreading process [8], and maximizing positive influence while formulating opinions [9].

Broadly speaking, most GNNs may be classified as either spectral or spatial. Spatial methods typically define convolution on graphs as a localized aggregation operator whereas spectral methods rely on the eigen-decomposition of a suitable graph Laplacian. The purpose of this paper is to introduce a novel spectral GNN for signed, directed graphs. While there have been several spatial GNNs [3, 10–12]

proposed for signed (and possibly directed) networks, this is one of the first works to propose a spectral GNN¹ for such networks.

A principal challenge in extending traditional spectral GNNs to this setting is to define a proper notion of the signed, directed graph Laplacian. Such a Laplacian should be positive semidefinite, have a bounded spectrum when properly normalized, and encode information about both the sign and direction of each edge. Here, we unify the magnetic Laplacian, which has been used in [14] to construct a GNN on an (unsigned) directed graph, with a signed Laplacian which has been used for a variety of data science tasks on (undirected) signed graphs[15–18]. Importantly, our proposed matrix, which we refer to as the *magnetic signed Laplacian*, reduces to either the magnetic Laplacian or the signed Laplacian when the graph is directed, but not signed, or signed, but not directed.

We show that our proposed *Magnetic Signed GNN (MSGNN)* is effective for a variety of node clustering and link prediction tasks. Specifically, we consider several variations of the link prediction task, some of which prioritize signed information over directional information, some of which prioritize directional information over signed information, while others emphasize the method’s ability to extract both signed and directional information simultaneously. This is in contrast to the concurrent preprint [13] which only considers undirected, signed tasks or unsigned, directed tasks.

In addition to testing MSGNN on established data sets, we also devise a novel synthetic model which we call the *Signed Directed Stochastic Block Model (SDSBM)*, which generalizes both the (undirected) Signed Stochastic Block Model from [12] and the (unsigned) Directed Stochastic Block Model from [5]. Analogous to these previous models, our SDSBM can be defined by a meta-graph structure and additional parameters describing density and noise levels. We also introduce a number of signed directed networks for link prediction tasks using lead-lag relationships in real-world financial time series.

Main Contributions. The main contributions of our work are as follows: (1) We devise a novel matrix operator called the magnetic signed Laplacian, which can naturally be applied to signed and directed networks, with desirable properties such as being Hermitian, positive semidefinite, and reducible to existing Laplacians when the network is unsigned and/or undirected. Moreover, the normalized version of this matrix has eigenvalues lying in $[0, 2]$. (2) We propose a spectral graph neural network architecture, MSGNN, based on this magnetic signed Laplacian, which attains leading performance on extensive node clustering and link prediction tasks, including novel tasks that consider edge sign and directionality jointly. To the best of our knowledge, this is the *first* work to evaluate GNNs² on tasks that are related to both edge sign and directionality. (3) We introduce a novel synthetic model for signed and directed networks, called Signed Directed Stochastic Block Model (SDSBM), and also contribute a number of new real-world data sets constructed from lead-lag relationships of financial time series data.

2 Related Work

In this section, we review related work constructing neural networks for directed graphs and signed graphs. We refer the reader to [1] for more background information.

Several works have aimed to define neural networks on directed graphs by constructing various directed graph Laplacians and defining convolution as multiplication in the associated eigenbasis. [19] defines a directed graph Laplacian by generalizing identities involving the undirected graph Laplacian and the stationary distribution of a random walk. [20] uses a similar idea, but with PageRank in place of a random walk. [21] constructs three different first- and second-order symmetric adjacency matrices and uses these adjacency matrices to define associated Laplacians. Similarly, [22] uses several different graph Laplacians based on various graph motifs.

Quite closely related to our work, [14] constructs a graph neural network using the magnetic Laplacian. Indeed, in the case where all links are positive, our GNN exactly reduces to the one proposed in [14]. Importantly, unlike the other directed graph Laplacians mentioned here, the magnetic Laplacian is a

¹We are aware only of one concurrent preprint [13], discussed thoroughly later, which was posted to arxiv.org recently (May 26, 2022), against which we have also compared in our experiments.

²Some previous work, such as [3], evaluates GNNs on signed and directed graphs. However, they focus on tasks where either only signed information is important, or where only directional information is important.

complex Hermitian matrix rather than a real, symmetric matrix. We also note [5], which constructs a GNN for node clustering on directed graphs based on flow imbalance.

All of the above works are restricted to unsigned graphs, i.e., graphs with positive edge weights. However, there are also a number of neural networks introduced for signed (and possibly also directed) graphs, mostly focusing on the task of link sign prediction, i.e., predicting whether a link between two nodes will be positive or negative. [23] is one of the first graph neural network methods to be applicable to signed networks, using an approach based on balance theory [24]. However, its design is mainly aimed at undirected graphs. [10] utilizes a graph attention mechanism based on [25] to learn node embeddings for signed directed graphs, using a novel motif-based GNN architecture based on balance theory and status theory [26]. Subsequently, [3] builds upon this work by increasing its efficiency and proposing a new objective function. In a similar vein, [11] also proposes a signed graph neural network for link sign prediction based on a novel objective function. In a different line of work, [12] proposes a GNN, not based on balance theory, designed for semi-supervised node clustering in signed (and possibly directed) graphs. We are aware of a concurrent preprint [13] which also constructs a GNN, SigMaNet, based on a signed magnetic Laplacian. Notably, the signed magnetic Laplacian considered in [13] is different from the magnetic signed Laplacian proposed here. The claimed advantage of SigMaNet is that it does not require the tuning of a charge parameter q and is invariant to, e.g., doubling the weight of every edge. In our work (as in [14]), we simply set $q = 0.25$, except for when the graph is undirected (in which case we set $q = 0$). However, a user may choose to also tune q through a standard cross-validation procedure (as in [14]). Moreover, one can readily address the latter issue by normalizing the adjacency matrix via a preprocessing step (see, for example, [27]).

We note that in the case where the graph is not signed but is weighted and directed, the matrix proposed in [13] does not reduce to the magnetic Laplacian considered in [14]. For example, denoting the graph adjacency matrix by \mathbf{A} , consider the case where $0 < \mathbf{A}_{j,i} < \mathbf{A}_{i,j}$. Let $m = \frac{1}{2}(\mathbf{A}_{i,j} + \mathbf{A}_{j,i})$, $\delta = \mathbf{A}_{i,j} - \mathbf{A}_{j,i}$, and let i denote the imaginary unit. Then the (i, j) -th entry of the matrix \mathbf{L}^σ proposed in [13] is given by $\mathbf{L}_{i,j}^\sigma = mi$, whereas the corresponding entry of the unnormalized magnetic Laplacian is given by $(\mathbf{L}_U^{(q)})_{i,j} = m \exp(2\pi i q \delta)$.

Additionally, we note that while SigMaNet is in principle well-defined on signed and directed graphs, the experiments in [13] are restricted to tasks where only signed or directional information is important (but not both). In our experiments, we will show that our proposed method outperforms SigMaNet on a variety of tasks on signed and/or directed networks. Moreover, we observe that the signed magnetic Laplacian \mathbf{L}^σ proposed in [13] satisfies an undesirable property — a node is assigned to have degree zero if it has an equal number of positive and negative connections (in the case where the graph is unweighted) — while our proposed Laplacian does not suffer from this issue.

3 Proposed Method

3.1 Problem Formulation

Let $\mathcal{G} = (\mathcal{V}, \mathcal{E}, w, \mathbf{X}_V)$ denote a signed, and possibly directed, weighted graph with node attributes, where \mathcal{V} is the set of nodes (or vertices), \mathcal{E} is the set of (directed) edges (or links), and $w : \mathcal{E} \rightarrow (-\infty, \infty) \setminus \{0\}$ is the weighting function. Let $\mathcal{E}^+ = \{e \in \mathcal{E} : w(e) > 0\}$ denote the set of positive edges and let $\mathcal{E}^- = \{e \in \mathcal{E} : w(e) < 0\}$ denote the set of negative edges so that $\mathcal{E} = \mathcal{E}^+ \cup \mathcal{E}^-$. Here, we do allow self loops but not multiple edges. That is, if $v_i, v_j \in \mathcal{V}$, there is at most one edge $e \in \mathcal{E}$ from v_i to v_j . Let $n = |\mathcal{V}|$, and let d_{in} be the number of attributes at each node so that \mathbf{X}_V is an $n \times d_{in}$ matrix whose rows are the attributes of each node. We let $\mathbf{A} = (A_{ij})_{i,j \in \mathcal{V}}$ denote the weighted, signed adjacency matrix where $\mathbf{A}_{i,j} = w_{i,j}$ if $(v_i, v_j) \in \mathcal{E}$, and $\mathbf{A}_{i,j} = 0$ otherwise.

3.2 Magnetic Signed Laplacian

In this section, we define Hermitian matrices $\mathbf{L}_U^{(q)}$ and $\mathbf{L}_N^{(q)}$ which we refer to as the unnormalized and normalized magnetic signed Laplacian matrices, respectively. In particular, when the graph \mathcal{G} is directed, but not signed, $\mathbf{L}_U^{(q)}$ and $\mathbf{L}_N^{(q)}$ reduce to the magnetic Laplacians utilized in works such as [14, 28, 29] and [30]. Similarly, when \mathcal{G} is signed, but not directed, $\mathbf{L}_U^{(q)}$ and $\mathbf{L}_N^{(q)}$ reduce to the signed Laplacian matrices considered in e.g., [15, 18] and [31]. Additionally, when the graph is neither signed nor directed, they reduce to the standard normalized and unnormalized graph Laplacians.

We first define a symmetrized adjacency matrix and a corresponding absolute degree matrix by considering

$$\tilde{\mathbf{A}}_{i,j} := \frac{1}{2}(\mathbf{A}_{i,j} + \mathbf{A}_{j,i}), \quad 1 \leq i, j \leq n,$$

$$\tilde{\mathbf{D}}_{i,i} := \frac{1}{2} \sum_{j=1}^n (|\mathbf{A}_{i,j}| + |\mathbf{A}_{j,i}|), \quad 1 \leq i \leq n,$$

with $\tilde{\mathbf{D}}_{i,j} = 0$ for $i \neq j$. Importantly, the use of absolute values ensures that the entries of $\tilde{\mathbf{D}}$ are non-negative. Furthermore, it ensures that all $\tilde{\mathbf{D}}_{i,i}$ will be strictly positive if the graph is connected. This is in contrast to the construction in [13] which will give a node degree zero if it has an equal number of positive and negative neighbors (for unweighted networks). To capture directional information, we next define a phase matrix $\Theta^{(q)}$ by

$$\Theta_{i,j}^{(q)} := 2\pi q(\mathbf{A}_{i,j} - \mathbf{A}_{j,i}),$$

where $q \in \mathbb{R}$ is the so-called “charge parameter”. In our experiments, for simplicity, we set $q = 0$ when the task at hand is unrelated to directionality, or when the underlying graph is undirected, and we set $q = 0.25$ for all the other tasks. We now construct a complex Hermitian matrix $\mathbf{H}^{(q)}$ by

$$\mathbf{H}^{(q)} := \tilde{\mathbf{A}} \odot \exp(i\Theta^{(q)}),$$

where \odot denotes elementwise multiplication and $\exp(i\Theta^{(q)})$ is defined elementwisely by $\exp(i\Theta^{(q)})_{i,j} := \exp(i\Theta_{i,j}^{(q)})$.

Note that $\mathbf{H}^{(q)}$ is Hermitian, as $\tilde{\mathbf{A}}$ is symmetric and $\Theta^{(q)}$ is skew-symmetric. In particular, when $q = 0$, we have $\mathbf{H}^{(0)} = \tilde{\mathbf{A}}$. Therefore, setting $q = 0$ is equivalent to making the input graph symmetric and discarding directional information. In general, however, $\mathbf{H}^{(q)}$ captures information about a link’s sign, through $\tilde{\mathbf{A}}$, and about its direction, through $\Theta^{(q)}$.

We observe that flipping the direction of an edge, i.e., replacing a positive or negative link from v_i to v_j with a link of the same sign from v_j to v_i corresponds to complex conjugation of $\mathbf{H}_{i,j}^{(q)}$ (assuming either that there is not already a link from v_j to v_i or that we also flip the direction of that link if there is one). We also note that if $q = 0.25$, $\mathbf{A}_{i,j} = \pm 1$, and $\mathbf{A}_{j,i} = 0$, we have

$$\mathbf{H}_{i,j}^{(0.25)} = \pm \frac{i}{2} = -\mathbf{H}_{j,i}^{(0.25)}.$$

Therefore, an edge from v_i to v_j with absolute weight one is treated as the opposite of an analogous edge from v_j to v_i .

Given the Hermitian matrix corresponding to a signed directed adjacency matrix, we define the unnormalized magnetic signed Laplacian by

$$\mathbf{L}_U^{(q)} := \tilde{\mathbf{D}} - \mathbf{H}^{(q)} = \tilde{\mathbf{D}} - \tilde{\mathbf{A}} \odot \exp(i\Theta^{(q)}), \quad (1)$$

and also define the normalized magnetic signed Laplacian by

$$\mathbf{L}_N^{(q)} := \mathbf{I} - \left(\tilde{\mathbf{D}}^{-1/2} \tilde{\mathbf{A}} \tilde{\mathbf{D}}^{-1/2} \right) \odot \exp(i\Theta^{(q)}). \quad (2)$$

Now we discuss some desirable properties that our proposed magnetic signed Laplacian matrices enjoy. Proofs of these theorems are provided in the appendix.

Theorem 1. *For any signed directed graph \mathcal{G} defined in Sec. 3.1, $\forall q \in \mathbb{R}$, both the unnormalized magnetic signed Laplacian $\mathbf{L}_U^{(q)}$ and its normalized counterpart $\mathbf{L}_N^{(q)}$ are positive semidefinite.*

Theorem 2. *For any signed directed graph \mathcal{G} defined in Sec. 3.1, $\forall q \in \mathbb{R}$, the eigenvalues of the normalized magnetic signed Laplacian $\mathbf{L}_N^{(q)}$ are contained in the interval $[0, 2]$.*

By construction, $\mathbf{L}_U^{(q)}$ and $\mathbf{L}_N^{(q)}$ are Hermitian, and Theorem 1 shows they are in addition positive semidefinite. Thus, they are diagonalizable by an orthonormal basis of complex eigenvectors $\mathbf{u}_1, \dots, \mathbf{u}_n$ associated to real, nonnegative eigenvalues $\lambda_1 \leq \dots \leq \lambda_n = \lambda_{\max}$. Thus, similar to the traditional normalized Laplacian, we may factor $\mathbf{L}_N^{(q)} = \mathbf{U} \Lambda \mathbf{U}^\dagger$, where \mathbf{U} is an $n \times n$ matrix whose k -th column is \mathbf{u}_k , for $1 \leq k \leq n$, Λ is a diagonal matrix with $\Lambda_{k,k} = \lambda_k$, and \mathbf{U}^\dagger is the conjugate transpose of \mathbf{U} . A similar formula holds for $\mathbf{L}_U^{(q)}$.

3.3 Spectral Convolution via the Magnetic Signed Laplacian

In this section, we show how to use a Hermitian, positive semidefinite matrix \mathbf{L} such as the normalized or unnormalized magnetic signed Laplacian introduced in Sec. 3.2, to defining convolution on a signed directed graph. This method is similar to the ones proposed for unsigned (possibly directed) graphs in, e.g., [32] and [14], but we provide details in order to keep our work reasonably self-contained.

Given \mathbf{L} , let $\mathbf{u}_1, \dots, \mathbf{u}_n$ be an orthonormal basis of eigenvectors such that $\mathbf{L}\mathbf{u}_k = \lambda_k \mathbf{u}_k$, and let \mathbf{U} be an $n \times n$ matrix whose k -th column is \mathbf{u}_k , for $1 \leq k \leq n$. For a signal $\mathbf{x} : \mathcal{V} \rightarrow \mathbb{C}$, we define its Fourier transform $\widehat{\mathbf{x}} \in \mathbb{C}^n$ by $\widehat{\mathbf{x}}(k) = \langle \mathbf{x}, \mathbf{u}_k \rangle := \mathbf{u}_k^\dagger \mathbf{x}$, and equivalently, $\widehat{\mathbf{x}} = \mathbf{U}^\dagger \mathbf{x}$.

Since \mathbf{U} is unitary, we readily obtain the Fourier inversion formula

$$\mathbf{x} = \mathbf{U}\widehat{\mathbf{x}} = \sum_{k=1}^n \widehat{\mathbf{x}}(k) \mathbf{u}_k. \quad (3)$$

Analogous to the well-known convolution theorem in Euclidean domains, we define the convolution of \mathbf{x} with a filter \mathbf{y} as multiplication in the Fourier domain, i.e., $\widehat{\mathbf{y}} * \widehat{\mathbf{x}}(k) = \widehat{\mathbf{y}}(k) \widehat{\mathbf{x}}(k)$. By (3), this implies $\mathbf{y} * \mathbf{x} = \mathbf{U}\text{Diag}(\widehat{\mathbf{y}})\widehat{\mathbf{x}} = (\mathbf{U}\text{Diag}(\widehat{\mathbf{y}})\mathbf{U}^\dagger)\mathbf{x}$, where $\text{Diag}(\mathbf{z})$ denotes a diagonal matrix with the vector \mathbf{z} on its diagonal. Therefore, we declare that \mathbf{Y} is a *generalized convolution matrix* if

$$\mathbf{Y} = \mathbf{U}\Sigma\mathbf{U}^\dagger, \quad (4)$$

for a diagonal matrix Σ . This is a natural generalization of the class of convolutions used in [33].

Some potential drawbacks exist to define convolution via (4). For one thing, it requires one to compute the eigen-decomposition of \mathbf{L} which is expensive for large graphs. For another, the number of trainable parameters is the size of the graph, rendering GNNs constructed via (4) prone to overfitting. To remedy these issues, we follow [34] (see also [35]) and observe that spectral convolution may also be implemented in the spatial domain via polynomials of \mathbf{L} by setting Σ equal to a polynomial of Λ . This reduces the number of trainable parameters from the size of the graph to the degree of the polynomial and also enhances robustness against perturbations [36]. As in [34], we let $\tilde{\Lambda} = \frac{2}{\lambda_{\max}}\Lambda - \mathbf{I}$ denote the normalized eigenvalue matrix (with entries in $[-1, 1]$) and choose

$$\Sigma = \sum_{k=0}^K \theta_k T_k(\tilde{\Lambda}),$$

for some $\theta_1, \dots, \theta_K \in \mathbb{R}$ where for $0 \leq k \leq K$, T_k is the Chebyshev polynomials defined by $T_0(x) = 1$, $T_1(x) = x$, and $T_k(x) = 2xT_{k-1}(x) + T_{k-2}(x)$ for $k \geq 2$. Since \mathbf{U} is unitary, we have $(\mathbf{U}\tilde{\Lambda}\mathbf{U}^\dagger)^k = \mathbf{U}\tilde{\Lambda}^k\mathbf{U}^\dagger$ for all k and therefore

$$\mathbf{Y}\mathbf{x} = \mathbf{U} \sum_{k=0}^K \theta_k T_k(\tilde{\Lambda}) \mathbf{U}^\dagger \mathbf{x} = \sum_{k=0}^K \theta_k T_k(\tilde{\Lambda}) \mathbf{x}, \quad (5)$$

where $\tilde{\Lambda} := \frac{2}{\lambda_{\max}}\Lambda - \mathbf{I}$. This is the class of convolutional filters we will use in our experiments. However, we note that if one desired, they could also imitate Sec. 3.1 on [14] to produce a class of filters based on [32] rather than [34].

It is important to note that $\tilde{\Lambda}$ is constructed so that the value of $(\mathbf{Y}\mathbf{x})_i$ depends on all nodes which can be reached within k -hops from v_i on the undirected, unsigned counterpart of \mathcal{G} , i.e. the graph whose adjacency matrix is given by $\mathbf{A}'_{i,j} = \frac{1}{2}(|\mathbf{A}_{i,j}| + |\mathbf{A}_{j,i}|)$. Therefore, this notion of convolution does not favor “outgoing neighbors” $\{v_j \in \mathcal{V} : (v_i, v_j) \in \mathcal{E}\}$ over “incoming neighbors” $\{v_j \in \mathcal{V} : (v_j, v_i) \in \mathcal{E}\}$ (or vice versa). This is important since for a given node v_i , both sets may contain different, useful information. Furthermore, since the phase matrix $\Theta^{(q)}$ encodes an outgoing edge and an incoming edge differently, the filter matrix \mathbf{Y} is also able to aggregate information from these two sets in different ways.

For computational complexity, while the matrix $\exp(i\Theta^{(q)})$ is dense in theory, one only needs to compute a small fraction of its entries corresponding to the nonzero entries of $\tilde{\Lambda}$ (which is sparse for most real-world data sets) in practice. Thus, the computational complexity of the convolution proposed here is equivalent to that of its undirected, unsigned counterparts.

3.4 The MSGNN architecture

In this section, we define our graph neural network architecture MSGNN. Let L denote the number of convolution layers in our GNN, and let $\mathbf{X}^{(0)}$ be an $n \times F_0$ input matrix with columns $\mathbf{x}_1^{(0)}, \dots, \mathbf{x}_{F_0}^{(0)}$. As in [14], we use a complex version of the Rectified Linear Unit defined by $\sigma(z) = z$, if $-\pi/2 \leq \arg(z) < \pi/2$, and $\sigma(z) = 0$ otherwise, where $\arg(\cdot)$ is the complex argument of $z \in \mathbb{C}$. Let F_ℓ be the number of channels in the ℓ -th layer. For $1 \leq \ell \leq L$, $1 \leq i \leq F_{\ell-1}$, and $1 \leq j \leq F_\ell$, let $\mathbf{Y}_{ij}^{(\ell)}$ be a convolution matrix defined by (4) or (5). Given the $(\ell-1)$ -st layer hidden representation matrix $\mathbf{X}^{(\ell-1)}$, we define $\mathbf{X}^{(\ell)}$ columnwise by

$$\mathbf{x}_j^{(\ell)} = \sigma \left(\sum_{i=1}^{F_{\ell-1}} \mathbf{Y}_{ij}^{(\ell)} \mathbf{x}_i^{(\ell-1)} + \mathbf{b}_j^{(\ell)} \right), \quad (6)$$

where $\mathbf{b}_j^{(\ell)}$ is a bias vector with equal real and imaginary parts $\text{Real}(\mathbf{b}_j^{(\ell)}) = \text{Imag}(\mathbf{b}_j^{(\ell)})$. In matrix form we write $\mathbf{X}^{(\ell)} = \mathbf{Z}^{(\ell)}(\mathbf{X}^{(\ell-1)})$, where $\mathbf{Z}^{(\ell)}$ is a hidden layer of the form (6). In our experiments, we utilize convolutions of the form (5) with $\mathbf{L} = \mathbf{L}_N^{(q)}$ and set $K = 1$, in which case we obtain

$$\mathbf{X}^{(\ell)} = \sigma \left(\mathbf{X}^{(\ell-1)} \mathbf{W}_{\text{self}}^{(\ell)} + \tilde{\mathbf{L}}_N^{(q)} \mathbf{X}^{(\ell-1)} \mathbf{W}_{\text{neigh}}^{(\ell)} + \mathbf{B}^{(\ell)} \right),$$

where $\mathbf{W}_{\text{self}}^{(\ell)}$ and $\mathbf{W}_{\text{neigh}}^{(\ell)}$ are learned weight matrices corresponding to the filter weights of different channels, and $\mathbf{B}^{(\ell)} = (\mathbf{b}_1^{(\ell)}, \dots, \mathbf{b}_{F_\ell}^{(\ell)})$. After the convolutional layers, we unwind the complex $n \times F_L$ matrix $\mathbf{X}^{(L)}$ into a real-valued $n \times 2F_L$ matrix. For node clustering, we then apply a linear layer by right-multiplication with a $2F_L \times C$ weight matrix $\mathbf{W}^{(L+1)}$, where C is the number of classes, followed by the softmax function. By default, we set $L = 2$, for which our MSGNN architecture is given by

$$\text{softmax}(\text{unwind}(\mathbf{Z}^{(2)}(\mathbf{Z}^{(1)}(\mathbf{X}^{(0)}))) \mathbf{W}^{(3)}).$$

For link prediction, we apply the same method through the unwind layer, and then concatenate the rows corresponding to pairs of nodes to obtain the edge features before the final linear layer and the softmax function.

4 Experiments

4.1 Tasks and Evaluation Metrics

4.1.1 Node Clustering

In the node clustering task, one aims to partition the nodes of the graph into C disjoint sets $\mathcal{C}_0, \dots, \mathcal{C}_{C-1}$ such that $\mathcal{V} = \mathcal{C}_0 \cup \mathcal{C}_1 \cup \dots \cup \mathcal{C}_{C-1}$. Typically in an unsigned, undirected network, one aims to choose the \mathcal{C}_i 's so that there are many links within each cluster and comparably few links between clusters, in which case nodes within each cluster are *similar* due to dense connections. In general, however, *similarity* could be defined differently [37]. In a signed graph, clusters can be formed by grouping together nodes with positive links and separating nodes with negative links, see [12]. In a directed graph, clusters can also be determined by a directed flow on the network, see [5]. More generally, we can define clusters based on an underlying meta-graph, where meta-nodes, each of which corresponds to a cluster in the network, can be distinguished based on either signed or directional information (e.g., flow imbalance [5]). This general meta-graph idea motivates our introduction of a novel synthetic network model, which we will define in Sec. 4.2.2, driven by both link sign and directionality. All of our node clustering experiments are done in the semi-supervised setting, where one selects a fraction of the nodes in each cluster as seed nodes, with known cluster membership labels. In all of our node clustering tasks, we measure our performance using the Adjusted Rand Index (ARI) [38].

4.1.2 Link Prediction

On undirected, unsigned graphs, link prediction is simply the task of predicting whether or not there is a link between a pair of nodes. Here, we consider five different variations of the link prediction

task for *signed and/or directed* networks. In our first task, link sign prediction (SP), one assumes that there is a link from v_i to v_j and aims to predict whether that link is positive or negative, i.e., whether $(v_i, v_j) \in \mathcal{E}^+$ or $(v_i, v_j) \in \mathcal{E}^-$. Our second task, direction prediction (DP), one aims to predict whether $(v_i, v_j) \in \mathcal{E}$ or $(v_j, v_i) \in \mathcal{E}$ under the assumption that exactly one of these two conditions holds. We also consider three-, four-, and five-class prediction problems. In the three-class problem (3C), the possibilities are $(v_i, v_j) \in \mathcal{E}$, $(v_j, v_i) \in \mathcal{E}$, or that neither (v_i, v_j) nor (v_j, v_i) are in \mathcal{E} . For the four-class problem (4C), the possibilities are $(v_i, v_j) \in \mathcal{E}^+$, $(v_i, v_j) \in \mathcal{E}^-$, $(v_j, v_i) \in \mathcal{E}^+$, and $(v_j, v_i) \in \mathcal{E}^-$. For the five-class problem (5C), we also add in the possibility that neither (v_i, v_j) nor (v_j, v_i) are in \mathcal{E} . For all tasks, we evaluate the performance with classification accuracy. For the first task, link sign prediction, we additionally measure our performance using Area Under Curve (AUC) [39], which is common practice in works concerning signed graphs. Notably, while (SP), (DP), and (3C) only require a method to be able to extract signed *or* directed information, the tasks (4C) and (5C) require it to be able to effectively process both sign *and* directional information.

4.2 Synthetic Data for Node Clustering

4.2.1 Established Synthetic Models

We conduct experiments on the Signed Stochastic Block Models (SSBMs) and polarized SSBMs (POL-SSBMs) models introduced in [12]. Notably, both of these models are signed, but undirected. In the SSBM(n, C, p, ρ, η) model, n represents the number of nodes, C is the number of clusters, p is the probability that there is a link (of either sign) between two nodes, ρ is the approximate ratio between the largest cluster size and the smallest cluster size, and η is the probability that an edge will have the “wrong” sign, i.e., that an intra-cluster edge will be negative or an inter-cluster edge will be positive. POL-SSBM (n, r, p, ρ, η, N) is a hierarchical variation of the SSBM model consisting of r communities, each of which is itself an SSBM. We refer the reader to [12] for details of both models.

4.2.2 Novel Synthetic Model: Signed Directed Stochastic Block Model (SDSBM)

A signed directed stochastic block model (SDSBM) relies on a meta-graph adjacency matrix $\mathbf{F} = (\mathbf{F}_{k,l})_{k,l=0,\dots,C-1}$, edge sparsity level p , the number of nodes n , and on a sign flip noise level parameter $0 \leq \eta \leq 0.5$.

An SDSBM model, denoted by SDSBM ($\mathbf{F}, n, p, \rho, \eta$), is built as follows:

- 1) Assign block sizes $n_0 \leq n_1 \leq \dots \leq n_{C-1}$ based on a parameter $\rho \geq 1$, which approximately represents the ratio between the size of largest block and the size of the smallest block. We choose ρ_0 such that $\rho_0^{C-1} = \rho$ and let n_0 be the largest integer such that $\sum_{i=0}^{C-1} \rho_0^i n_0 \leq n$. We let $n_i = \lfloor \rho_0 n_{i-1} \rfloor$ for $i = 1, \dots, C-2$ and then set $n_{C-1} = n - \sum_{i=0}^{C-2} n_i$. By construction, we have $n_i \approx \rho_0 n_{i-1}$, and so we have $n_{C-1} \approx \rho_0^{C-1} n_0 = \rho n_0$.
- 2) Assign each node to one of the C blocks, so that each block C_i has size n_i .
- 3) For nodes $v_i \in \mathcal{C}_k$, and $v_j \in \mathcal{C}_l$, independently sample an edge from v_i to v_j with probability $p \cdot |\mathbf{F}_{k,l}|$. Give this edge weight 1 if $F_{k,l} \geq 0$ and weight -1 if $F_{k,l} < 0$.
- 4) Flip the sign of all the edges in the generated graph with sign flip probability η .

In our experiments, we use two sets of specific meta-graph structures $\{\mathbf{F}_1(\gamma)\}, \{\mathbf{F}_2(\gamma)\}$, with three and four clusters, respectively, where $0 \leq \gamma \leq 0.5$ is the directional noise level. Specifically, we are interested in SDSBM ($\mathbf{F}_1(\gamma), n, p, \rho, \eta$) and SDSBM ($\mathbf{F}_2(\gamma), n, p, \rho, \eta$) models with varying γ where

$$\mathbf{F}_1(\gamma) = \begin{bmatrix} 0.5 & \gamma & -\gamma \\ 1 - \gamma & 0.5 & -0.5 \\ -1 + \gamma & -0.5 & 0.5 \end{bmatrix},$$

$$\mathbf{F}_2(\gamma) = \begin{bmatrix} 0.5 & \gamma & -\gamma & -\gamma \\ 1 - \gamma & 0.5 & -0.5 & -\gamma \\ -1 + \gamma & -0.5 & 0.5 & -\gamma \\ -1 + \gamma & -1 + \gamma & -1 + \gamma & 0.5 \end{bmatrix}.$$

To better understand the above SDSBM models, we consider the following toy examples, illustrated in Fig. 1, regarding groups of athletes and sports fans on social media. Here, signed, directed edges

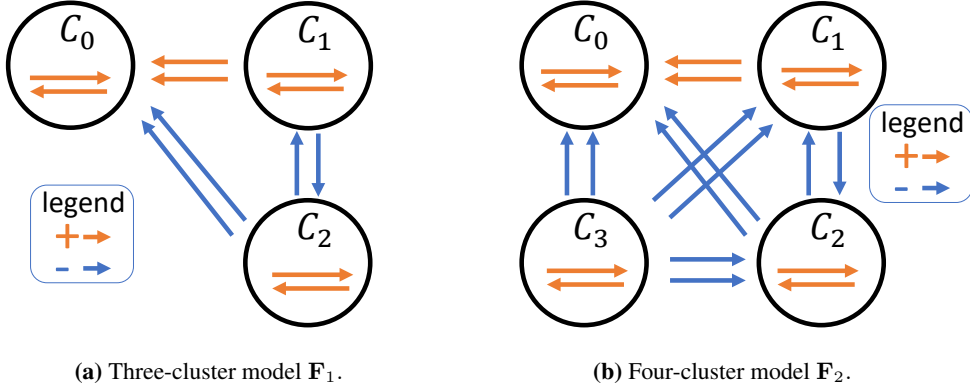


Figure 1: SDSBM illustration.

represent positive or negative mentions. In Fig. 1(a), \mathcal{C}_0 are the players of a sports team, \mathcal{C}_1 is a group of their fans who typically say positive things about the players, and \mathcal{C}_2 is a group of fans of a rival team, who typically say negative things about the players. Since they are fans of rival teams, the members of \mathcal{C}_1 and \mathcal{C}_2 both say negative things about each other. In general, fans mention the players more than players mention fans, which leads to net flow imbalance. In Fig. 1(b), we add in \mathcal{C}_3 , a group of fans of a third, less important team. This group dislikes the other two teams and disseminates negative content about \mathcal{C}_0 , \mathcal{C}_1 , and \mathcal{C}_2 . However, since this third team is quite unimportant, no one comments anything back.

Notably, in both examples, as the expected edge density is identical both within and across clusters, discarding either signed or directional information will ruin the clustering structure. For instance, in both examples, if we discard directional information, then \mathcal{C}_0 will look identical to \mathcal{C}_1 in the resulting meta-graph. On the other hand, if we discard signed information, \mathcal{C}_1 will look identical to \mathcal{C}_2 . We also note that the SDSBM model proposed here is a generalization of both the SSBM model from [12] and the Directed Stochastic Block Model from [5] when we have suitable meta-graph structures.

4.3 Real-World Data for Link Prediction

4.3.1 Standard Real-World Data Sets

We consider four standard real-world data sets. The first two, *BitCoin-Alpha* and *BitCoin-OTC* [2], which describe bitcoin trading, are both signed and directed. The latter two, *Slashdot* [40], which is related to a technology news website, and *Epinions* [41], which describes consumer reviews, are signed, but not directed. These networks range in size from 3783 to 131828 nodes.

4.3.2 Novel Financial Data Sets from Stock Returns

Using financial time series data, we build signed directed networks where the weighted edges encode lead-lag relationships inherent in the financial market, for each year in the interval 2000-2020. The lead-lag matrices are built from time series of daily price returns³. We refer to these networks as our **F**inancial **L**ead-**L**ag (FiLL) data sets. For each year in the data set, we build a signed directed graph (*FiLL-pvCLCL*) based on the price return of 444 stocks at market close times on consecutive days. We also build another graph (*FiLL-OPCL*), based on the price return of 430 stocks from market open to close. The difference between 444 versus 430 stems from the non-availability of certain open and close prices on some days for certain stocks. The lead-lag metric that is captured by the entry $A_{i,j}$ in each network encodes a measure that quantifies the extent to which stock v_i leads stock v_j , and is obtained by computing the linear regression coefficient when regressing the time series (of length 245) of daily returns of stock v_i against the lag-one version of the time series (of length 245) of the daily returns of stock v_j . Specifically, we use the beta coefficient of the corresponding simple linear regression, to serve as the one-day lead-lag metric. The resulting matrix is asymmetric and signed, rendering it amenable to a signed directed network interpretation. The initial matrix is dense, with nonzero entries outside the main diagonal, since we do not consider the own auto-correlation of each stock.

³Raw CRSP data accessed through <https://wrds-www.wharton.upenn.edu/>.

Table 1: Link sign prediction test performance comparison. The best is marked in **bold red** and the second best is marked in underline blue. Results are averaged over five runs with different data splits.

| Metric | Data Set | SGCN | SDGNN | SiGAT | SNEA | SSSNET | SigMaNet | MSGNN |
|----------|----------------------|-------------------|-------------------|-------------------|-------------------|-----------------------------------|-------------------|-----------------------------------|
| AUC | <i>BitCoin-Alpha</i> | 0.737 \pm 0.009 | 0.687 \pm 0.009 | 0.626 \pm 0.022 | 0.724 \pm 0.011 | 0.779\pm0.012 | 0.534 \pm 0.070 | <u>0.746\pm0.071</u> |
| | <i>BitCoin-OTC</i> | 0.740 \pm 0.015 | 0.743 \pm 0.017 | 0.661 \pm 0.023 | 0.693 \pm 0.018 | <u>0.813\pm0.025</u> | 0.517 \pm 0.071 | 0.829\pm0.060 |
| | <i>Slashdot</i> | 0.885 \pm 0.005 | 0.830 \pm 0.005 | 0.670 \pm 0.017 | 0.875 \pm 0.008 | 0.955\pm0.006 | 0.522 \pm 0.218 | <u>0.887\pm0.079</u> |
| | <i>Epinions</i> | 0.897 \pm 0.003 | 0.821 \pm 0.016 | 0.752 \pm 0.008 | 0.905 \pm 0.004 | 0.945\pm0.009 | 0.525 \pm 0.158 | <u>0.917\pm0.008</u> |
| accuracy | <i>BitCoin-Alpha</i> | 0.655 \pm 0.007 | 0.633 \pm 0.008 | 0.582 \pm 0.019 | 0.641 \pm 0.009 | <u>0.670\pm0.033</u> | 0.524 \pm 0.052 | 0.672\pm0.071 |
| | <i>BitCoin-OTC</i> | 0.679 \pm 0.015 | 0.674 \pm 0.008 | 0.619 \pm 0.025 | 0.628 \pm 0.012 | <u>0.732\pm0.023</u> | 0.510 \pm 0.055 | 0.750\pm0.052 |
| | <i>Slashdot</i> | 0.803 \pm 0.006 | 0.752 \pm 0.005 | 0.622 \pm 0.013 | 0.797 \pm 0.006 | <u>0.856\pm0.030</u> | 0.509 \pm 0.147 | <u>0.821\pm0.078</u> |
| | <i>Epinions</i> | 0.816 \pm 0.003 | 0.737 \pm 0.014 | 0.683 \pm 0.008 | 0.819 \pm 0.003 | 0.846\pm0.062 | 0.513 \pm 0.092 | <u>0.842\pm0.015</u> |

Next, we sparsify each network at a sparsity level of 0.2, keeping only 20% of the edges with the largest magnitudes. The resulting data sets are denoted by the type of return and the year. We denote them by “*FiLL-pvCLCL*”+“year”, or “*FiLL-OPCL*”+“year”, respectively, such as *FiLL-OPCL2017*. In our experiments, we also report the average results across the years for each type of the returns, where the data sets are denoted by *FiLL-pvCLCL* (avg.) and *FiLL-OPCL* (avg.), respectively. To facilitate future research using these data sets as benchmarks, both the dense lead-lag matrices and their sparsified counterparts will be made publicly available.

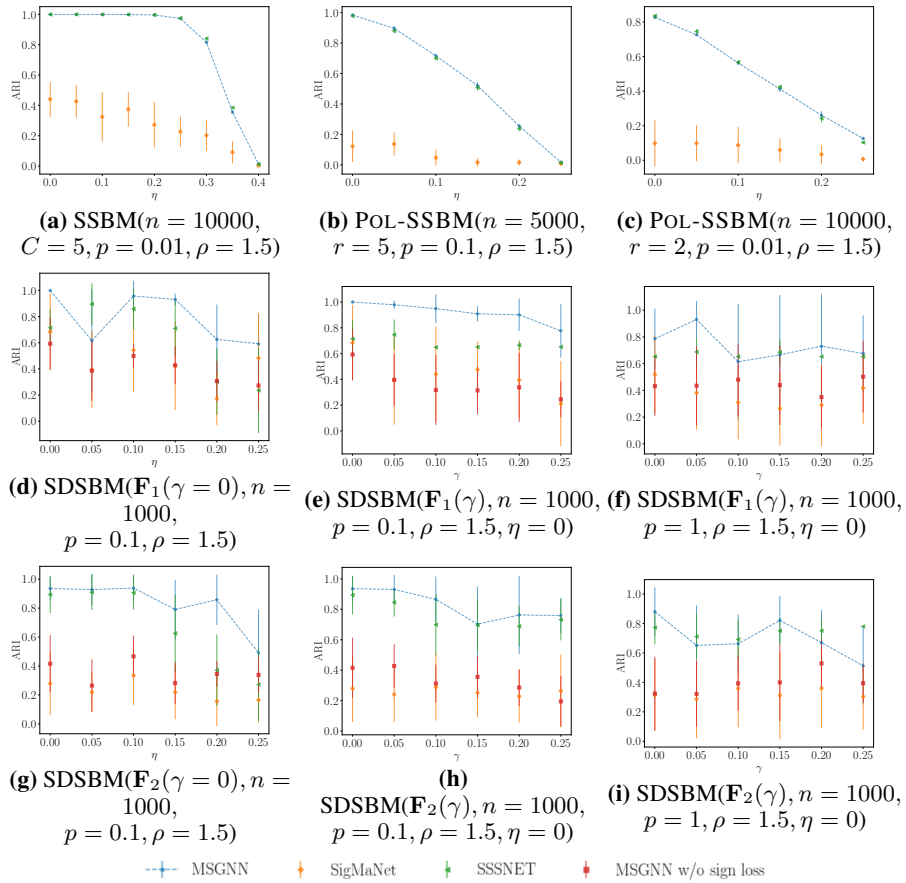


Figure 2: Node clustering test ARI comparison on synthetic data. Dashed lines highlight MSGNN’s performance. Error bars indicate one standard error. Results are averaged over ten runs — five different networks, each with two distinct data splits.

4.4 Methods to Compare Against

We compare MSGNN against representative GNNs from the literature. The six methods we consider are • 1) SGCN [23], • 2) SDGNN [3], • 3) SiGAT [10], • 4) SNEA [11], • 5) SSSNET [12], and • 6) SigMaNet [13]. For all link prediction tasks, comparisons are carried out on all baselines; for the

Table 2: Link prediction test accuracy comparison for directions (and signs). The best is marked in **bold red** and the second best is marked in underline blue. The link prediction tasks are introduced in Sec. 4.1.2.

| Data Set | Link Task | SGCN | SDGNN | SiGAT | SNEA | SSSNET | SigMaNet | MSGNN |
|---------------------------|-----------|-----------------------------------|-----------------------------------|-------------------|-----------------------------------|-----------------------------------|-------------------|-----------------------------------|
| <i>BitCoin-Alpha</i> | DP | 0.664\pm0.007 | 0.638 \pm 0.010 | 0.589 \pm 0.007 | 0.654 \pm 0.001 | 0.640 \pm 0.021 | 0.531 \pm 0.047 | 0.680\pm0.033 |
| | 3C | 0.783\pm0.006 | 0.752 \pm 0.015 | 0.718 \pm 0.012 | 0.751 \pm 0.005 | 0.562 \pm 0.151 | 0.432 \pm 0.132 | 0.779\pm0.035 |
| | 4C | 0.516 \pm 0.009 | 0.500 \pm 0.016 | 0.439 \pm 0.018 | 0.484 \pm 0.011 | 0.560\pm0.030 | 0.245 \pm 0.057 | 0.525\pm0.070 |
| | 5C | 0.761\pm0.005 | 0.726 \pm 0.011 | 0.707 \pm 0.010 | 0.722 \pm 0.004 | 0.625 \pm 0.072 | 0.194 \pm 0.099 | 0.746\pm0.029 |
| <i>BitCoin-OTC</i> | DP | 0.620 \pm 0.009 | 0.599 \pm 0.004 | 0.586 \pm 0.011 | 0.570 \pm 0.015 | 0.651\pm0.010 | 0.507 \pm 0.032 | 0.657\pm0.043 |
| | 3C | 0.785\pm0.002 | 0.744 \pm 0.010 | 0.697 \pm 0.010 | 0.769 \pm 0.006 | 0.661 \pm 0.041 | 0.314 \pm 0.060 | 0.796\pm0.010 |
| | 4C | 0.516\pm0.007 | 0.460 \pm 0.007 | 0.367 \pm 0.016 | 0.456 \pm 0.023 | 0.508\pm0.017 | 0.241 \pm 0.027 | 0.470 \pm 0.077 |
| | 5C | 0.760\pm0.002 | 0.721 \pm 0.007 | 0.686 \pm 0.006 | 0.750\pm0.008 | 0.655 \pm 0.033 | 0.171 \pm 0.020 | 0.723 \pm 0.018 |
| <i>FiLL-pvCLCL (avg.)</i> | DP | 0.542 \pm 0.001 | 0.851\pm0.004 | 0.542 \pm 0.002 | 0.540 \pm 0.002 | 0.851 \pm 0.007 | 0.521 \pm 0.033 | 0.879\pm0.015 |
| | 3C | 0.382 \pm 0.002 | 0.607\pm0.002 | 0.371 \pm 0.003 | 0.370 \pm 0.001 | 0.588 \pm 0.006 | 0.328 \pm 0.014 | 0.639\pm0.008 |
| | 4C | 0.380 \pm 0.001 | 0.635 \pm 0.010 | 0.385 \pm 0.003 | 0.376 \pm 0.002 | 0.759\pm0.003 | 0.255 \pm 0.022 | 0.771\pm0.006 |
| | 5C | 0.358 \pm 0.001 | 0.499 \pm 0.007 | 0.352 \pm 0.001 | 0.349 \pm 0.001 | 0.552\pm0.006 | 0.202 \pm 0.020 | 0.614\pm0.007 |
| <i>FiLL-OPCL (avg.)</i> | DP | 0.537 \pm 0.001 | 0.837\pm0.008 | 0.537 \pm 0.003 | 0.540 \pm 0.002 | 0.830 \pm 0.006 | 0.506 \pm 0.024 | 0.851\pm0.013 |
| | 3C | 0.377 \pm 0.001 | 0.591\pm0.004 | 0.367 \pm 0.001 | 0.366 \pm 0.002 | 0.553 \pm 0.013 | 0.328 \pm 0.008 | 0.623\pm0.006 |
| | 4C | 0.369 \pm 0.001 | 0.595 \pm 0.006 | 0.364 \pm 0.001 | 0.359 \pm 0.002 | 0.731\pm0.004 | 0.251 \pm 0.028 | 0.762\pm0.015 |
| | 5C | 0.358 \pm 0.000 | 0.471 \pm 0.004 | 0.348 \pm 0.000 | 0.349 \pm 0.001 | 0.528\pm0.005 | 0.209 \pm 0.010 | 0.582\pm0.010 |
| <i>FiLL-pvCLCL2002</i> | DP | 0.593 \pm 0.005 | 0.848 \pm 0.015 | 0.591 \pm 0.020 | 0.617 \pm 0.015 | 0.849\pm0.030 | 0.463 \pm 0.025 | 0.876\pm0.039 |
| | 3C | 0.420 \pm 0.007 | 0.596\pm0.011 | 0.399 \pm 0.014 | 0.425 \pm 0.005 | 0.580 \pm 0.026 | 0.320 \pm 0.049 | 0.640\pm0.002 |
| | 4C | 0.399 \pm 0.013 | 0.578 \pm 0.014 | 0.388 \pm 0.008 | 0.352 \pm 0.006 | 0.747\pm0.050 | 0.263 \pm 0.066 | 0.826\pm0.010 |
| | 5C | 0.368 \pm 0.003 | 0.469 \pm 0.013 | 0.368 \pm 0.009 | 0.352 \pm 0.004 | 0.538\pm0.030 | 0.183 \pm 0.064 | 0.618\pm0.044 |
| <i>FiLL-pvCLCL2009</i> | DP | 0.540 \pm 0.003 | 0.946 \pm 0.004 | 0.610 \pm 0.025 | 0.566 \pm 0.005 | 0.951\pm0.013 | 0.474 \pm 0.036 | 0.970\pm0.004 |
| | 3C | 0.403 \pm 0.002 | 0.742\pm0.012 | 0.407 \pm 0.021 | 0.403 \pm 0.005 | 0.721 \pm 0.035 | 0.344 \pm 0.051 | 0.744\pm0.032 |
| | 4C | 0.466 \pm 0.004 | 0.821 \pm 0.021 | 0.529 \pm 0.024 | 0.474 \pm 0.002 | 0.918\pm0.017 | 0.219 \pm 0.141 | 0.907\pm0.047 |
| | 5C | 0.398 \pm 0.002 | 0.702 \pm 0.016 | 0.401 \pm 0.019 | 0.395 \pm 0.001 | 0.737\pm0.023 | 0.192 \pm 0.105 | 0.771\pm0.012 |
| <i>FiLL-pvCLCL2016</i> | DP | 0.580 \pm 0.007 | 0.810 \pm 0.026 | 0.588 \pm 0.014 | 0.543 \pm 0.031 | 0.819\pm0.031 | 0.488 \pm 0.015 | 0.879\pm0.003 |
| | 3C | 0.405 \pm 0.004 | 0.577\pm0.006 | 0.385 \pm 0.015 | 0.372 \pm 0.002 | 0.567 \pm 0.023 | 0.327 \pm 0.055 | 0.620\pm0.009 |
| | 4C | 0.352 \pm 0.009 | 0.562 \pm 0.031 | 0.357 \pm 0.017 | 0.337 \pm 0.009 | 0.725\pm0.024 | 0.226 \pm 0.075 | 0.782\pm0.009 |
| | 5C | 0.374 \pm 0.002 | 0.441 \pm 0.015 | 0.357 \pm 0.003 | 0.358 \pm 0.006 | 0.490\pm0.043 | 0.188 \pm 0.049 | 0.566\pm0.045 |
| <i>FiLL-OPCL2002</i> | DP | 0.547 \pm 0.006 | 0.813 \pm 0.013 | 0.582 \pm 0.016 | 0.571 \pm 0.002 | 0.826\pm0.023 | 0.526 \pm 0.038 | 0.874\pm0.003 |
| | 3C | 0.397 \pm 0.003 | 0.592\pm0.011 | 0.403 \pm 0.010 | 0.390 \pm 0.014 | 0.563 \pm 0.025 | 0.332 \pm 0.035 | 0.630\pm0.006 |
| | 4C | 0.335 \pm 0.004 | 0.528 \pm 0.010 | 0.369 \pm 0.018 | 0.322 \pm 0.008 | 0.717\pm0.039 | 0.230 \pm 0.032 | 0.764\pm0.060 |
| | 5C | 0.369 \pm 0.002 | 0.458 \pm 0.007 | 0.361 \pm 0.009 | 0.348 \pm 0.005 | 0.558\pm0.028 | 0.246 \pm 0.076 | 0.612\pm0.007 |
| <i>FiLL-OPCL2009</i> | DP | 0.542 \pm 0.006 | 0.906 \pm 0.010 | 0.601 \pm 0.011 | 0.550 \pm 0.007 | 0.920\pm0.011 | 0.474 \pm 0.073 | 0.935\pm0.001 |
| | 3C | 0.389 \pm 0.006 | 0.663\pm0.002 | 0.408 \pm 0.005 | 0.380 \pm 0.003 | 0.616 \pm 0.015 | 0.308 \pm 0.028 | 0.688\pm0.004 |
| | 4C | 0.337 \pm 0.005 | 0.693 \pm 0.020 | 0.391 \pm 0.012 | 0.326 \pm 0.003 | 0.855\pm0.016 | 0.295 \pm 0.064 | 0.884\pm0.012 |
| | 5C | 0.380 \pm 0.004 | 0.551 \pm 0.032 | 0.364 \pm 0.007 | 0.374 \pm 0.003 | 0.621\pm0.028 | 0.161 \pm 0.019 | 0.604\pm0.131 |
| <i>FiLL-OPCL2016</i> | DP | 0.609 \pm 0.006 | 0.833 \pm 0.011 | 0.573 \pm 0.017 | 0.604 \pm 0.022 | 0.845\pm0.024 | 0.468 \pm 0.096 | 0.867\pm0.002 |
| | 3C | 0.416 \pm 0.002 | 0.558\pm0.014 | 0.388 \pm 0.014 | 0.367 \pm 0.003 | 0.531 \pm 0.063 | 0.343 \pm 0.042 | 0.606\pm0.003 |
| | 4C | 0.409 \pm 0.004 | 0.554 \pm 0.019 | 0.385 \pm 0.014 | 0.377 \pm 0.043 | 0.654\pm0.041 | 0.226 \pm 0.053 | 0.703\pm0.078 |
| | 5C | 0.356 \pm 0.002 | 0.429\pm0.022 | 0.347 \pm 0.003 | 0.352 \pm 0.001 | 0.400 \pm 0.082 | 0.241 \pm 0.078 | 0.503\pm0.043 |

Table 3: Link prediction test performance comparison for variants of MSGNN. Each variant is denoted by a 3-tuple: (q value, whether to include signed features, whether to include weighted features), where “T” and “F” stand for “True” and “False”, respectively. “T” for weighted features means simplying summing up entries in the adjacency matrix while “T” means summing the absolute values of the entries. The best is marked in **bold red** and the second best is marked in underline blue.

| Data Set | Link Task | (0, F, F) | (0, F, T) | (0, T, F) | (0, T, T) | (0, T, T) | (0.25, F, F) | (0.25, F, T) | (0.25, T, F) | (0.25, T, T) |
|---------------------------|-----------|-------------------|-------------------|-------------------|-----------------------------------|-----------------------------------|-------------------|-----------------------------------|-----------------------------------|-----------------------------------|
| <i>BitCoin-Alpha</i> | DP | 0.686 \pm 0.059 | 0.677 \pm 0.053 | 0.677 \pm 0.053 | 0.708\pm0.033 | 0.680 \pm 0.033 | 0.686 \pm 0.059 | 0.677 \pm 0.053 | 0.708\pm0.033 | 0.680 \pm 0.033 |
| | 3C | 0.801 \pm 0.037 | 0.786 \pm 0.036 | 0.770 \pm 0.035 | 0.813\pm0.003 | 0.770 \pm 0.026 | 0.805 \pm 0.018 | 0.778 \pm 0.035 | 0.781 \pm 0.035 | 0.818\pm0.008 |
| | 4C | 0.510 \pm 0.011 | 0.445 \pm 0.039 | 0.445 \pm 0.039 | 0.625\pm0.016 | 0.525 \pm 0.070 | 0.510 \pm 0.011 | 0.445 \pm 0.039 | 0.445 \pm 0.039 | 0.625\pm0.016 |
| | 5C | 0.758 \pm 0.004 | 0.716 \pm 0.019 | 0.716 \pm 0.019 | 0.784\pm0.011 | 0.738 \pm 0.031 | 0.740 \pm 0.023 | 0.716 \pm 0.019 | 0.718 \pm 0.023 | 0.788\pm0.007 |
| <i>FiLL-pvCLCL (avg.)</i> | DP | 0.878 \pm 0.009 | 0.871 \pm 0.014 | 0.876 \pm 0.014 | 0.878 \pm 0.009 | 0.866 \pm 0.019 | 0.879 \pm 0.013 | 0.883\pm0.007 | 0.881\pm0.012 | 0.874 \pm 0.010 |
| | 3C | 0.625 \pm 0.004 | 0.637 \pm 0.009 | 0.639 \pm 0.008 | 0.606 \pm 0.010 | 0.637 \pm 0.008 | 0.616 \pm 0.014 | 0.636 \pm 0.011 | 0.639\pm0.007 | 0.614 \pm 0.016 |
| | 4C | 0.617 \pm 0.010 | 0.623 \pm 0.008 | 0.628 \pm 0.010 | 0.759 \pm 0.014 | 0.783\pm0.013 | 0.608 \pm 0.013 | 0.625 \pm 0.010 | 0.629 \pm 0.004 | 0.744 \pm 0.011 |
| | 5C | 0.465 \pm 0.016 | 0.504 \pm 0.005 | 0.500 \pm 0.007 | 0.543 \pm 0.018 | 0.608\pm0.006 | 0.475 \pm 0.010 | 0.504 \pm 0.006 | 0.501 \pm 0.006 | 0.558 \pm 0.010 |

node clustering tasks, we only compare MSGNN against SSSNET and SigMaNet as adapting the other methods to this task is nontrivial due to their specific loss functions.

4.5 Implementation Details

Experiments were conducted on a compute node with 8 Nvidia Tesla T4, 96 Intel Xeon Platinum 8259CL CPUs @ 2.50GHz and 378GB RAM. Due to memory constraint, SDGNN and SiGAT have to be run on CPUs for *Slashdot* and *Epinions* while the others are on GPUs. Among the signed GNNs, SDGNN is the least efficient method in terms of speed and space complexity, followed by SiGAT, as both methods need to count motifs. MSGNN is generally the fastest and also space friendly. For example, the average training time for a financial link task are 200s for SGCN, 1500s for SDGNN, 150s for SNEA, 500s for SiGAT, 50s for SSSNET, 120s for SigMaNet, and **40s** for MSGNN, respectively. Averaged results are reported with error bars representing one standard deviation in the figures, and plus/minus one standard deviation in the tables. For all the experiments, we use Adam [42] as our optimizer with learning rate 0.01 and employ ℓ_2 regularization with weight decay parameter $5 \cdot 10^{-4}$ to avoid overfitting. We use the open-source library PyTorch Geometric Signed

Directed [1] for data loading, node and edge splitting, node feature preparation, and implementation of some baselines. For SSSNET [12], we use hidden size 16, 2 hops, and $\tau = 0.5$, and we adapt the architecture so that SSSNET is suitable for link prediction tasks. For SigMaNet [13], we use the code and parameter settings from <https://anonymous.4open.science/r/SigMaNet>. We set the number of layers to two for all methods. Anonymous codes and some preprocessed data are available at <https://anonymous.4open.science/r/MSGNN>.

4.5.1 Node Clustering

We conduct semi-supervised node clustering, with 10% of all nodes from each cluster as test nodes, 10% as validation nodes to select the model, and the remaining 80% as training nodes (10% of which are seed nodes). For each of the synthetic models, we first generate five different networks, each with two different data splits, then conduct experiments on them and report average performance over these 10 runs. To train the GNNs on the signed undirected data sets (SSBMs and POL-SSBMs), we use the semi-supervised loss function $\mathcal{L}_1 = \mathcal{L}_{\text{PBNC}} + \gamma_s(\mathcal{L}_{\text{CE}} + \gamma_t \mathcal{L}_{\text{triplet}})$ as in [12], with the same hyperparameter setting $\gamma_s = 50$, $\gamma_t = 0.1$, where $\mathcal{L}_{\text{PBNC}}$ is the self-supervised probabilistic balanced normalized cut loss function penalizing unexpected signs. For these signed undirected graphs, we use validation ARI for early stopping. For the SDSBMs, our loss function is the sum of \mathcal{L}_1 and the imbalance loss function $\mathcal{L}_{\text{vol_sum}}^{\text{sort}}$ from [5] (absolute edge weights as input), i.e., $\mathcal{L}_2 = \mathcal{L}_{\text{vol_sum}}^{\text{sort}} + \mathcal{L}_1$, and we use the self-supervised part of the validation loss ($\mathcal{L}_{\text{PBNC}} + \mathcal{L}_{\text{vol_sum}}^{\text{sort}}$) for early stopping. We further restrict the GNNs to be trained on the subgraph induced by only the training nodes while applying the training loss function. For MSGNN on SDSBMs, we set $q = 0.25$ to emphasize directionality. The input node feature matrix \mathbf{X}_V for undirected signed networks in our experiments is generated by stacking the eigenvectors corresponding to the largest C eigenvalues of a regularized version of the symmetrized adjacency matrix $\tilde{\mathbf{A}}$. For signed directed networks, we calculate the in- and out-degrees based on both signs to obtain a four-dimensional feature vector for each node. We train all GNNs for the node clustering task for at most 1000 epochs with a 200-epoch early-stopping scheme.

4.5.2 Link Prediction

We train all GNNs for each link prediction task for 200 epochs. We use the proposed loss functions from their original papers for SGCN [23], SNEA [11], SiGAT [10], and SDGNN [3], and we use cross-entropy loss \mathcal{L}_{CE} for SigMaNet [13], SSSNET [12] and MSGNN. For all link prediction experiments, we sample 20% edges as test edges, and use the rest of the edges for training. Five splits were generated randomly for each input graph. We calculate the in- and out-degrees based on both signs from the observed input graph (removing test edges) to obtain a four-dimensional feature vector for each node for training SigMaNet [13], SSSNET [12], and MSGNN, and we use the default settings from [1] for SGCN [23], SNEA [11], SiGAT [10], and SDGNN [3].

4.6 Experimental Results

4.6.1 Node Clustering

Fig. 2 compares the node clustering performance of MSGNN with two other signed GNNs on synthetic data, and additionally against a variant of MSGNN on SDSBMs which discards the $\mathcal{L}_{\text{PBNC}}$ part of the self-supervised loss function that takes edge signs into account, i.e., the loss is $\mathcal{L}_3 = \mathcal{L}_{\text{vol_sum}}^{\text{sort}} + \gamma_s(\mathcal{L}_{\text{CE}} + \gamma_t \mathcal{L}_{\text{triplet}})$. Error bars are given by one standard error. We conclude that MSGNN outperforms SigMaNet on all data sets and is competitive with SSSNET. On most data sets, MSGNN achieves leading performance, whereas on the others it is slightly outperformed by SSSNET, depending on the network density, noise level, network size, and the underlying meta-graph structure. Comparing the two MSGNN variants, we conclude that the edge sign information in these SDSBM models plays a vital role since MSGNN outperforms MSGNN w/o sign loss in all cases.

4.6.2 Link Prediction

We display our results for SP in Table 1 and our results for tasks DP, 3C, 4C, and 5C in Table 2. For SP, we see that our method, MSGNN, has the highest accuracy on two of four data sets and the second highest accuracy on the other two. It also has the highest AUC on one of the four data sets and the second highest on the other three. For tasks DP, 3C, 4C, and 5C, MSGNN is clearly the top performing method, achieving the highest level of accuracy in thirty-three out of forty total cases.

For financial data sets, we report the average performance across the 21 yearly networks (marked with “avg.”) for both types of returns, and for individual networks every seven years; due to space, only three years are reported. Specifically, the “avg.” results for the two novel financial data sets first average the accuracy values across the 21 years for each run, then report the mean and standard deviation over the five runs.⁴

4.6.3 Discussion

We now discuss the influence of the magnetic part in the Laplacian matrix as well as how input features affect the performance. Table 3 compares different variants of MSGNN on the link prediction tasks DP, 3C, 4C, and 5C, with respect to whether we use a traditional signed Laplacian that is initially designed for undirected networks (in which case we have $q = 0$) and a magnetic signed Laplacian that strongly emphasizes directionality (in which case we have $q = 0.25$), whether to include sign in input node features (if we set this to be False, then we have only in- and out-degrees computed just like in [14] regardless of edge signs), and whether we take edge weights into account (if False, we view all edge weights as having magnitude one). We conclude that incorporating directionality in the Laplacian matrix (i.e., having nonzero q) typically leads to better performance in these directionality-related tasks, but given in- and out-degree node features, the undirected variants (with $q = 0$) could also occasionally perform well. Besides, signed features are often helpful for tasks involving sign prediction. Finally, the consideration of edge weights is usually disadvantageous if we are not considering edge signs, while its effect on performance is unclear when edge signs have already been considered in node features. Note that, by default, the degree calculated given signed edge weights are net degrees, meaning that we sum the edge weights up without taking absolute values. The features that sum up absolute values of edge weights are denoted with T’ in the table.

5 Conclusion and Outlook

In this paper, we propose a spectral graph neural network based on a novel magnetic signed Laplacian matrix, introduce a novel synthetic network model and new real-world data sets, and conduct experiments on node clustering and link prediction tasks that are not restricted to considering either link sign or directionality alone. In future work, we plan to investigate an extension of our work to temporal/dynamic graphs, where node features and/or edge information could evolve over time [43, 44]. We are also interested in extending our work to being able to encode nontrivial edge features, and to hypergraphs as well as other complex network structures.

References

- [1] Yixuan He, Xitong Zhang, Junjie Huang, Benedek Rozemberczki, Mihai Cucuringu, and Gesine Reinert. PyTorch Geometric Signed Directed: A Survey and Software on Graph Neural Networks for Signed and Directed Graphs. *arXiv preprint arXiv:2202.10793*, 2022. [1](#), [2](#), [11](#)
- [2] Srijan Kumar, Francesca Spezzano, VS Subrahmanian, and Christos Faloutsos. Edge weight prediction in weighted signed networks. In *2016 IEEE 16th International Conference on Data Mining (ICDM)*, pages 221–230. IEEE, 2016. [1](#), [8](#)
- [3] Junjie Huang, Huawei Shen, Liang Hou, and Xueqi Cheng. SDGNN: Learning Node Representation for Signed Directed Networks. In *Proceedings of the AAAI Conference on Artificial Intelligence*, volume 35, pages 196–203, 2021. [1](#), [2](#), [3](#), [9](#), [11](#)
- [4] Stefanos Bennett, Mihai Cucuringu, and Gesine Reinert. Detection and clustering of lead-lag networks for multivariate time series with an application to financial markets. *7th SIGKDD Workshop on Mining and Learning from Time Series (MiLeTS)*, 2021. [1](#)
- [5] Yixuan He, Gesine Reinert, and Mihai Cucuringu. DIGRAC: Digraph Clustering Based on Flow Imbalance. *arXiv preprint arXiv:2106.05194*, 2021. [1](#), [2](#), [3](#), [6](#), [8](#), [11](#)
- [6] Yixuan He, Quan Gan, David Wipf, Gesine Reinert, Junchi Yan, and Mihai Cucuringu. GNRank: Learning Global Rankings from Pairwise Comparisons via Directed Graph Neural Networks. *arXiv preprint arXiv:2202.00211*, 2022. [1](#)

⁴For certain years, some baseline cannot generate results when the input networks are too dense for some negative sampling within the training loss to work. We treat these entries as missing and average over the remaining years.

[7] Quan Zheng, David B Skillicorn, and Olivier Walther. Signed directed social network analysis applied to group conflict. In *2015 IEEE International Conference on Data Mining Workshop (ICDMW)*, pages 1007–1014. IEEE, 2015. 1

[8] Jiangping Hu and Wei Xing Zheng. Bipartite consensus for multi-agent systems on directed signed networks. In *52nd IEEE Conference on decision and control*, pages 3451–3456. IEEE, 2013. 1

[9] Weijia Ju, Ling Chen, Bin Li, Wei Liu, Jun Sheng, and Yuwei Wang. A new algorithm for positive influence maximization in signed networks. *Information Sciences*, 512:1571–1591, 2020. 1

[10] Junjie Huang, Huawei Shen, Liang Hou, and Xueqi Cheng. Signed graph attention networks. In *International Conference on Artificial Neural Networks*, pages 566–577. Springer, 2019. 1, 3, 9, 11

[11] Yu Li, Yuan Tian, Jiawei Zhang, and Yi Chang. Learning signed network embedding via graph attention. In *Proceedings of the AAAI Conference on Artificial Intelligence*, volume 34, pages 4772–4779, 2020. 3, 9, 11

[12] Yixuan He, Gesine Reinert, Songchao Wang, and Mihai Cucuringu. SSSNET: Semi-Supervised Signed Network Clustering. In *Proceedings of the 2022 SIAM International Conference on Data Mining (SDM)*, pages 244–252. SIAM, 2022. 1, 2, 3, 6, 7, 8, 9, 11

[13] Stefano Fiorini, Stefano Coniglio, Michele Ciavotta, and Enza Messina. SigMaNet: One Laplacian to Rule Them All. *arXiv preprint arXiv:2205.13459*, 2022. 2, 3, 4, 9, 11

[14] Xitong Zhang, Yixuan He, Nathan Brugnone, Michael Perlmutter, and Matthew Hirn. Magnet: A neural network for directed graphs. *Advances in Neural Information Processing Systems*, 34, 2021. 2, 3, 5, 6, 12

[15] Jérôme Kunegis, Stephan Schmidt, Andreas Lommatzsch, Jürgen Lerner, Ernesto W De Luca, and Sahin Albayrak. Spectral analysis of signed graphs for clustering, prediction and visualization. In *Proceedings of the 2010 SIAM international conference on data mining*, pages 559–570. SIAM, 2010. 2, 3

[16] Quan Zheng and David B Skillicorn. Spectral embedding of signed networks. In *Proceedings of the 2015 SIAM international conference on data mining*, pages 55–63. SIAM, 2015.

[17] Pedro Mercado, Francesco Tudisco, and Matthias Hein. Clustering signed networks with the geometric mean of Laplacians. *Advances in neural information processing systems*, 29, 2016.

[18] Mihai Cucuringu, Apoorv Vikram Singh, Deborah Sulem, and Hemant Tyagi. Regularized spectral methods for clustering signed networks. *Journal of Machine Learning Research*, 22(264):1–79, 2021. URL <http://jmlr.org/papers/v22/20-1289.html>. 2, 3

[19] Yi Ma, Jianye Hao, Yaodong Yang, Han Li, Junqi Jin, and Guangyong Chen. Spectral-based graph convolutional network for directed graphs. *arXiv:1907.08990*, 2019. 2

[20] Zekun Tong, Yuxuan Liang, Changsheng Sun, Xinkie Li, David Rosenblum, and Andrew Lim. Digraph Inception Convolutional Networks. In *NeurIPS*, 2020. 2

[21] Zekun Tong, Yuxuan Liang, Changsheng Sun, David S. Rosenblum, and Andrew Lim. Directed graph convolutional network. *arXiv:2004.13970*, 2020. 2

[22] Federico Monti, Karl Otness, and Michael M. Bronstein. Motifnet: A motif-based graph convolutional network for directed graphs. In *2018 IEEE Data Science Workshop*, pages 225–228, 2018. 2

[23] Tyler Derr, Yao Ma, and Jiliang Tang. Signed graph convolutional networks. In *2018 IEEE International Conference on Data Mining (ICDM)*, pages 929–934. IEEE, 2018. 3, 9, 11

[24] Frank Harary. On the notion of balance of a signed graph. *Michigan Mathematical Journal*, 2(2):143–146, 1953. 3

[25] Petar Veličković, Guillem Cucurull, Arantxa Casanova, Adriana Romero, Pietro Lio, and Yoshua Bengio. Graph attention networks. *arXiv preprint arXiv:1710.10903*, 2017. 3

[26] Jure Leskovec, Daniel Huttenlocher, and Jon Kleinberg. Signed networks in social media. In *Proceedings of the SIGCHI conference on human factors in computing systems*, pages 1361–1370, 2010. 3

[27] Alexander Cloninger. A note on Markov normalized magnetic eigenmaps. *Applied and Computational Harmonic Analysis*, 43(2):370 – 380, 2017. ISSN 1063-5203. doi: <https://doi.org/10.1016/j.acha.2016.11.002>. 3

[28] Michaël Fanuel, Carlos M Alaiz, and Johan AK Suykens. Magnetic eigenmaps for community detection in directed networks. *Physical Review E*, 95(2):022302, 2017. 3

[29] Michaël Fanuel, Carlos M. Alaíz, Ángela Fernández, and Johan A.K. Suykens. Magnetic eigenmaps for the visualization of directed networks. *Applied and Computational Harmonic Analysis*, 44:189–199, 2018. 3

[30] Bruno Messias F. de Resende and Luciano da F. Costa. Characterization and comparison of large directed networks through the spectra of the magnetic Laplacian. *Chaos: An Interdisciplinary Journal of Nonlinear Science*, 30(7):073141, 2020. 3

[31] Fatihcan M. Atay and Hande Tunçel. On the spectrum of the normalized Laplacian for signed graphs: Interlacing, contraction, and replication. *Linear Algebra and its Applications*, 442: 165–177, 2014. ISSN 0024-3795. doi: <https://doi.org/10.1016/j.laa.2013.08.022>. URL <https://www.sciencedirect.com/science/article/pii/S0024379513005211>. Special Issue on Spectral Graph Theory on the occasion of the Latin Ibero-American Spectral Graph Theory Workshop (Rio de Janeiro, 27-28 September 2012). 3

[32] Thomas N. Kipf and Max Welling. Semi-Supervised Classification with Graph Convolutional Networks. In *International Conference on Learning Representations (ICLR)*, 2017. 5

[33] Joan Bruna, Wojciech Zaremba, Arthur Szlam, and Yann LeCun. Spectral Networks and Deep Locally Connected Networks on Graphs. In *International Conference on Learning Representations (ICLR)*, 2014. 5

[34] Michaël Defferrard, Xavier Bresson, and Pierre Vandergheynst. Convolutional Neural Networks on Graphs with Fast Localized Spectral Filtering. In *Advances in Neural Information Processing Systems 29*, pages 3844–3852, 2016. 5

[35] David K Hammond, Pierre Vandergheynst, and Rémi Gribonval. Wavelets on graphs via spectral graph theory. *Applied and Computational Harmonic Analysis*, 30(2):129–150, 2011. 5

[36] Ron Levie, Wei Huang, Lorenzo Bucci, Michael M Bronstein, and Gitta Kutyniok. Transferability of spectral graph convolutional neural networks. *arXiv preprint arXiv:1907.12972*, 2019. 5

[37] Yixuan He. GNNs for Node Clustering in Signed and Directed Networks. In *Proceedings of the Fifteenth ACM International Conference on Web Search and Data Mining*, pages 1547–1548, 2022. 6

[38] Lawrence Hubert and Phipps Arabie. Comparing partitions. *Journal of Classification*, 2(1): 193–218, 1985. 6

[39] Andrew P Bradley. The use of the area under the roc curve in the evaluation of machine learning algorithms. *Pattern Recognition*, 30(7):1145–1159, 1997. 7

[40] Bruno Ordozgoiti, Antonis Matakos, and Aristides Gionis. Finding Large Balanced Subgraphs in Signed Networks. In *Proceedings of The Web Conference 2020*, WWW '20, page 1378–1388, New York, NY, USA, 2020. Association for Computing Machinery. ISBN 9781450370233. doi: [10.1145/3366423.3380212](https://doi.org/10.1145/3366423.3380212). 8

[41] Paolo Massa and Paolo Avesani. Controversial users demand local trust metrics: An experimental study on opinions. com community. In *AAAI*, pages 121–126, 2005. 8

[42] Diederik P Kingma and Jimmy Ba. Adam: A method for stochastic optimization. *arXiv preprint arXiv:1412.6980*, 2014. 10

[43] Quang-Vinh Dang and Claudia-Lavinia Ignat. Link-sign prediction in dynamic signed directed networks. In *2018 IEEE 4th International Conference on Collaboration and Internet Computing (CIC)*, pages 36–45. IEEE, 2018. 12

[44] Benedek Rozemberczki, Paul Scherer, Yixuan He, George Panagopoulos, Alexander Riedel, Maria Astefanoaei, Oliver Kiss, Ferenc Beres, Guzmán López, Nicolas Collignon, et al. Pytorch geometric temporal: Spatiotemporal signal processing with neural machine learning models. In *Proceedings of the 30th ACM International Conference on Information & Knowledge Management*, pages 4564–4573, 2021. 12

A Appendix

B Proof of Theorems

B.1 Proof of Theorem 1

Proof. Let $\mathbf{x} \in \mathbb{C}^n$. Since $\mathbf{L}_U^{(q)}$ is Hermitian, we have $\text{Imag}(\mathbf{x}^\dagger \mathbf{L}_U^{(q)} \mathbf{x}) = 0$. Next, we note by the triangle inequality that $\tilde{\mathbf{D}}_{i,i} = \frac{1}{2} \sum_{j=1}^n (|\mathbf{A}_{i,j}| + |\mathbf{A}_{j,i}|) \geq \sum_{j=1}^n |\tilde{\mathbf{A}}_{i,j}|$. Therefore, we may use the fact that $\tilde{\mathbf{A}}$ is symmetric to obtain

$$\begin{aligned} & 2\text{Real} \left(\mathbf{x}^\dagger \mathbf{L}_U^{(q)} \mathbf{x} \right) \\ &= 2 \sum_{i=1}^n \tilde{\mathbf{D}}_{i,i} |\mathbf{x}(i)|^2 - 2 \sum_{i,j=1}^n \tilde{\mathbf{A}}_{i,j} \mathbf{x}(i) \overline{\mathbf{x}(j)} \cos(\Theta_{i,j}^{(q)}) \\ &\geq 2 \sum_{i,j=1}^n |\tilde{\mathbf{A}}_{i,j}| |\mathbf{x}(i)|^2 - 2 \sum_{i,j=1}^n |\tilde{\mathbf{A}}_{i,j}| |\mathbf{x}(i)| |\mathbf{x}(j)| \\ &= \sum_{i,j=1}^n |\tilde{\mathbf{A}}_{i,j}| (|\mathbf{x}(i)| - |\mathbf{x}(j)|)^2 \geq 0. \end{aligned}$$

Thus, $\mathbf{L}_U^{(q)}$ is positive semidefinite. For the normalized magnetic Laplacian, one may verify $(\tilde{\mathbf{D}}^{-1/2} \tilde{\mathbf{A}} \tilde{\mathbf{D}}^{-1/2}) \odot \exp(i\Theta^{(q)}) = \tilde{\mathbf{D}}^{-1/2} (\tilde{\mathbf{A}} \odot \exp(i\Theta^{(q)})) \tilde{\mathbf{D}}^{-1/2}$, and hence

$$\mathbf{L}_N^{(q)} = \tilde{\mathbf{D}}^{-1/2} \mathbf{L}_U^{(q)} \tilde{\mathbf{D}}^{-1/2}. \quad (7)$$

Thus, letting $\mathbf{y} = \tilde{\mathbf{D}}^{-1/2} \mathbf{x}$, the fact that $\tilde{\mathbf{D}}$ is diagonal implies

$$\mathbf{x}^\dagger \mathbf{L}_N^{(q)} \mathbf{x} = \mathbf{x}^\dagger \tilde{\mathbf{D}}^{-1/2} \mathbf{L}_U^{(q)} \tilde{\mathbf{D}}^{-1/2} \mathbf{x} = \mathbf{y}^\dagger \mathbf{L}_U^{(q)} \mathbf{y} \geq 0. \quad \square$$

B.2 Proof of Theorem 2

Proof. By Theorem 1, it suffices to show that the lead eigenvalue, λ_n , is less than or equal to 2. The Courant-Fischer theorem shows that $\lambda_n = \max_{\mathbf{x} \neq 0} \frac{\mathbf{x}^\dagger \mathbf{L}_N^{(q)} \mathbf{x}}{\mathbf{x}^\dagger \mathbf{x}}$. Therefore, using (7) and setting $\mathbf{y} = \tilde{\mathbf{D}}^{-1/2} \mathbf{x}$, we have

$$\lambda_n = \max_{\mathbf{x} \neq 0} \frac{\mathbf{x}^\dagger \tilde{\mathbf{D}}^{-1/2} \mathbf{L}_U^{(q)} \tilde{\mathbf{D}}^{-1/2} \mathbf{x}}{\mathbf{x}^\dagger \mathbf{x}} = \max_{\mathbf{y} \neq 0} \frac{\mathbf{y}^\dagger \mathbf{L}_U^{(q)} \mathbf{y}}{\mathbf{y}^\dagger \tilde{\mathbf{D}} \mathbf{y}}.$$

First, we observe that since $\tilde{\mathbf{D}}$ is diagonal, we have

$$\mathbf{y}^\dagger \tilde{\mathbf{D}} \mathbf{y} = \sum_{i=1}^n \tilde{\mathbf{D}}_{i,i} |\mathbf{y}(i)|^2 = \frac{1}{2} \sum_{i,j=1}^n (|\mathbf{A}_{i,j}| + |\mathbf{A}_{j,i}|) |\mathbf{y}(i)|^2.$$

The triangle inequality implies that $|\tilde{\mathbf{A}}_{i,j}| \leq \frac{1}{2} (|\mathbf{A}_{i,j}| + |\mathbf{A}_{j,i}|)$. Therefore, we may repeatedly expand the sums and interchange the roles of i and j to obtain

$$\begin{aligned} & \mathbf{y}^\dagger \mathbf{L}_U^{(q)} \mathbf{y} \\ & \leq \frac{1}{2} \sum_{i,j=1}^n (|\mathbf{A}_{i,j}| + |\mathbf{A}_{j,i}|) |\mathbf{y}(i)|^2 + \frac{1}{2} \sum_{i,j=1}^n (|\mathbf{A}_{i,j}| + |\mathbf{A}_{j,i}|) |\mathbf{y}(i)| |\mathbf{y}(j)| \\ &= \frac{1}{2} \sum_{i,j=1}^n |\mathbf{A}_{i,j}| (|\mathbf{y}(i)| + |\mathbf{y}(j)|)^2 \leq \sum_{i,j=1}^n |\mathbf{A}_{i,j}| (|\mathbf{y}(i)|^2 + |\mathbf{y}(j)|^2) \\ &= \sum_{i,j=1}^n (|\mathbf{A}_{i,j}| + |\mathbf{A}_{j,i}|) |\mathbf{y}(i)|^2 = 2\mathbf{y}^\dagger \tilde{\mathbf{D}} \mathbf{y}. \end{aligned} \quad \square$$